Low-Energy Electron-Diffraction Intensity Calculations for Beryllium with a Realistic Crystal Potential*

J. A. Strozier, Jr.
Department of Materials Science, State University of New York at Stony Brook, Stony Brook, New York 11790†
and Department of Materials Science and Engineering, Cornell University, Ithaca, New York 14850

and

R. O. Jones‡
Laboratory of Atomic and Solid State Physics, Cornell University, Ithaca, New York 14850
(Received 19 August 1970)

The band-matching approach is used to calculate low-energy electron-diffraction intensity-voltage curves for the basal cleavage plane of beryllium. An approximation to the exact theory, made possible by the presence of strong inelastic scattering, enables these curves to be calculated very rapidly, for general angles of incidence and with a detailed nonlocal potential. The potential is constructed from first principles, includes thermal and inelastic-scattering effects, and has no adjustable parameters. Over a wide range of incident angles the calculated curves show marked agreement with recent experiments. A test of the sensitivity of the calculations to changes in the scattering potential parameters shows that the absolute intensity, rather than peak position or peak width, should be the best experimental probe of the scattering processes. A new approximation for core-valence exchange is used in the calculation and is described in an appendix.

I. INTRODUCTION

The description of structural and other physical properties of surfaces requires a detailed knowledge of the electronic and ionic charge distributions in the outermost atomic layers. Owing, in part, to the short penetration depth, which limits the sampling region to near the surface, the most promising probe of these quantities is low-energy electron diffraction (LEED). Recent advances in experimental techniques and the consequent availability of data from clean surfaces have revived theoretical interest in the problem, and this promises to provide a basis from which structural information about the surface can be obtained from LEED data. Correlation with other measurements of surface and bulk properties should result.

The first theoretical description of electron diffraction was given by Bethe,[1] whose wave-matching approach has been the prototype for a number of subsequent calculations. This method, in which the logarithmic derivative of the wave function inside the crystal is matched at the surface to appropriate plane-wave states, was used by Morse[2] and by Kronig and Penney[3] for simple one-dimensional potentials, and the results reproduced certain features of the experiments of Davisson and Germer.[4] Consideration of inelastic scattering was formally included by Slater[5] and by Molière,[6] who included the effect through an imaginary term in the Fourier component of the potential. Some of the recently developed formalisms for the scattering of electrons at surfaces follow the approach of Bethe, and each may generally be classified as either dynamical or kinematical in nature.

Dynamical theories emphasize the self-consistent scattering between atoms and layers of atoms. This approach requires a detailed knowledge of the scattering potential, sometimes expressed in terms of phase shifts, and has been adopted by several workers.[7-19] In principle it is exact, but the complexity of the calculation has limited numerical calculations to extremely simple model potentials (or very few phase shifts) or to a single angle of incidence. For purely elastic-scattering potentials, dynamical theories lead to intensity-voltage curves of the form shown schematically in Fig. 1(a). At energies corresponding to absolute band gaps in the bulk, the reflectivity is unity and the peak widths are of the order of an electron volt. This is in marked contradiction with experimental findings,[20] and Duke and Tucker,[21] who extended the purely elastic analysis of Beeby,[13] and Jones and Strozier[22] have shown that it is essential to include inelastic scattering at the outset.

On the other hand, kinematical theory ignores multiple scattering between atoms, but notes that strong inelastic scattering will restrict the scattering region to near the surface.[23] The approach has been used by a number of workers to discuss experimental results.[24-26] The experimental features of low reflectivities and broad peak widths follow naturally from a kinematical approach [see the schematic curve in Fig. 1(c)]. Furthermore, the

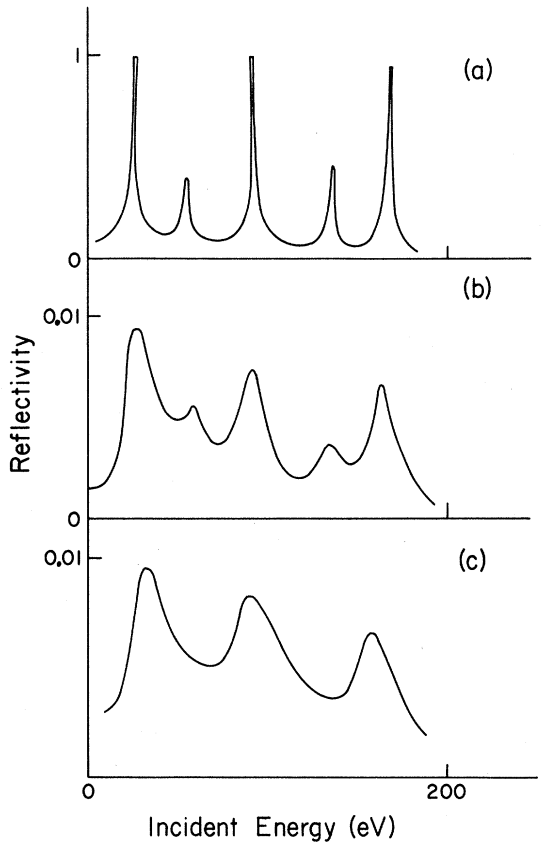

FIG. 1. Schematic intensity-voltage curves for (a) dynamical calculation without inelastic scattering, (b) experiment, (c) kinematical calculation with absorption. Note the change in reflectivity scale. The dynamical calculations lead to maximum reflectivities of unity, typically two orders of magnitude greater than experiment or than kinematical calculations with appropriate absorption.

secondary peaks in LEED spectra, generally attributed to multiple scattering, are less prominent than the Bragg peaks. The kinematical theory seems, therefore, to be an appropriate starting point,[27] to which multiple-scattering effects may be added as perturbations.

In this paper, we describe an exact scattering formalism based on the wave-matching approach as developed by Heine[28] and further amplified by Boudreaux and Heine[10] and by Capart.[16] The physical evidence of strong inelastic and relatively weak elastic scattering suggests an approximation to the exact theory which includes multiple-scattering effects consistently to second order. The method has important advantages over existing approaches. (a) It is applicable with a detailed, nonlocal potential and inelastic effects may be included in a systematic way. (b) It is valid for arbitrary angles of incidence. (c) The calculations proceed very rapidly, enabling us to examine the sensitivity of the resulting intensity-voltage curves to both the elastic and inelastic parts in the scattering potential. Finally, we calculate the diffracted intensities of the specularly reflected (00) beam from the (0001) face of beryllium as a function of incident energy and angle and compare them with recent experimental results. The calculated intensities show marked agreement with the experimental data over a wide range of incident angles.

In Sec. II, the matching equations in matrix notation are derived. The results are similar to Capart's and are included, not only for completeness, but to emphasize the differences, which reflect the perturbation calculation of the Bloch states adopted here. In Sec. III, these equations are used to obtain an exact expression describing the LEED scattering process as a series of terms of increasing order. Each term is given a physical meaning. The series is truncated to second order in a consistent way in Sec. IV. This approximation is used for the calculations presented here. The pseudopotential used is described in Sec. V, and in Sec. VI the results are compared with the experimental work of Baker.[29]

II. MATCHING FORMULATION

The wave-matching approach may be summarized as follows. Plane-wave states are constructed outside the crystal which conserve the incident beam energy and momentum parallel to the surface. Bloch states are calculated inside the crystal which conserve the same quantities. The matching of the logarithmic derivatives of the two sets of states at the surface generates a set of linear equations whose solutions give the amplitudes of the various beams inside and outside the crystal. Implicit in this model is the assumption that the surface divides space into two regions: (a) the bulk, in which the potential is everywhere three dimensionally periodic; (b) the vacuum, in which it is everywhere zero. As it stands, this description does not allow variations in the potential from bulk values near the surface. A discussion of the way these effects may be incorporated in the wave-matching approach is given in Sec. VI.

A. Wave Field Outside Crystal

The solutions of the Schrödinger equation in vacuum are plane waves whose energy is given by the square of the wave vector. In particular, the incident electron is represented by $e^{i\vec{K}\cdot\vec{r}}$. For convenience, the wave vector $\vec{K}$ is separated into components parallel ($\vec{K}^{\parallel}$) and perpendicular ($\vec{K}^{\perp}$) to the surface. The coordinates of the system are chosen such that the crystal surface is the plane $z = 0$, with the z direction positive inside the crystal. If the angle between the incident wave vector $\vec{K}$ and the surface normal is denoted by θ and the energy by E,

$|\vec{K}^{\perp}| = E\cos\theta$ and $|\vec{K}^{\parallel}| = E\sin\theta$.

(Atomic units are used throughout. The unit of energy is the rydberg and distances are expressed in terms of Bohr radii.) The potential, three dimensional inside the crystal and zero outside, has two-dimensional periodicity *everywhere*, and scatters the incident electron into all plane waves

$$\psi_i^0 = \exp[i(-\vec{k}_i^{\perp} + \vec{K}^{\parallel} + \vec{g}_i^{\parallel})\cdot\vec{r}] , \tag{1}$$

which conserve energy and crystal momentum parallel to the surface up to the surface projection of a reciprocal-lattice vector $\vec{g}_{\perp}^{\parallel}$.[30] The perpendicular component of the ith scattered wave $\vec{k}_i^{\perp}$, the parallel component of the ith reciprocal-lattice vector, and the energy are all related by energy conservation

$$|\vec{k}_i^{\perp}| = (E - |\vec{K}^{\parallel} + \vec{g}_i^{\parallel}|^2)^{1/2} . \tag{2}$$

The positive square root is taken to satisfy the boundary condition at minus infinity (i.e., one plane wave, the incident wave, propagates towards the crystal). For a given energy, the scattered waves can be grouped into a finite set of propagating waves with $\vec{k}_i^{\perp}$ real and an infinite set of evanescent waves with $\vec{k}_i^{\perp}$ imaginary. Writing the total wave field Ψ^0 outside as a linear combination of the incident and all possible scattered waves, we have

$$\Psi^0 = e^{i\vec{K}\cdot\vec{r}} + \sum_i A_i \psi_i^0 . \tag{3}$$

The sum runs over all distinct $\vec{g}_i^{\parallel}$. The solution of the problem consists of finding the complex amplitudes A_i of the scattered waves.

B. Wave Field Inside Crystal

Inside the crystal, the two dimensionally periodic potential scatters the incident wave into all possible *Bloch* waves which conserve energy and crystal momentum parallel to the surface. The jth such Bloch state can be written

$$\psi_j^B = \exp[i(\vec{k}_j'^{\perp} + \vec{K}^{\parallel} + \vec{g}_j^{\parallel})\cdot\vec{r}]\, u_j(\vec{r}) . \tag{4}$$

We expand the periodic factor $u_j(\vec{r})$ in plane waves

$$u_j(\vec{r}) = 1 + \sum_l{}' B_j(\vec{g}_l) e^{i\vec{g}_l\cdot\vec{r}} . \tag{5}$$

The sum is over all nonzero three-dimensional reciprocal-lattice vectors $\vec{g}_l$. This form is chosen so that the Bloch function resembles a perturbation expansion, in keeping with our later use of perturbation theory in evaluating the Bloch states. Formally, both the expansion coefficients $B_j(\vec{g}_l)$ and the perpendicular component of the wave vector $\vec{k}_j'^{\perp}$ can be determined by solving the secular equation derived from the Schrödinger equation for the crystal potential V,

$$(-\nabla^2 + V)\psi_j^B = E\psi_j^B . \tag{6}$$

The total wave field inside is thus a linear combination of all such Bloch waves $\Psi^I = \sum_j C_j \psi_j^B$. The unknown C_j's may be regarded as transmission coefficients.

C. Matching at Surface

Matching the wave fields and their derivatives at the surface generates the set of linear equations relating the unknown A_i's and C_j's to the Bloch wave expansion coefficients and the internal and external wave vectors. The matching of the wave fields

$$\Psi^0\big|_{z=0} = \Psi^I\big|_{z=0}$$

leads to

$$e^{i(\vec{K}^{\parallel}\cdot\vec{r})} + \sum_i A_i e^{i(\vec{K}^{\parallel} + \vec{g}_i^{\parallel})\cdot\vec{r}} = \sum_j C_j e^{i(\vec{K}^{\parallel} + \vec{g}_j^{\parallel})\cdot\vec{r}} \left[1 + \sum_l{}' B_j(\vec{g}_l) e^{i(\vec{g}_l^{\parallel}\cdot\vec{r})}\right] . \tag{7}$$

It is convenient to replace each reciprocal-lattice vector in the sum on l by its components parallel and perpendicular to the surface, $\vec{g}_l = \vec{g}_m^{\parallel} + \vec{g}_{mn}^{\perp}$. Thus,

$$\sum_l{}' B_j(\vec{g}_l) e^{i\vec{g}_l^{\parallel}\cdot\vec{r}} = \sum_m e^{i\vec{g}_m^{\parallel}\cdot\vec{r}} \sum_n{}'' B_j(m,n) , \tag{8}$$

where the double prime denotes the exclusion of the term corresponding to $\vec{g}_k = 0$. The index n runs along each reciprocal-lattice rod defined by $\vec{g}_m^{\parallel}$, i.e., over all reciprocal-lattice vectors having the same parallel component $\vec{g}_m^{\parallel}$. Note that the notation for the expansion coefficients has been simplified as follows: $B_j(m,n) \equiv B_j(\vec{g}_m^{\parallel} + g_{m,n}^{\perp})$. We now define $D_{j,m} \equiv \sum_n{}'' B_j(m,n)$.

Linear independence allows Eq. (7) to be written as a set of linear equations (one for each value of i)

$$(100..)^T \delta_{i0} + A_i = C_i + \sum_j C_j D_{j,i-j} , \tag{9}$$

where T indicates the corresponding column vector. Similarly, the matching of the normal derivatives at the surface,

$$\left.\frac{\partial\Psi^0}{\partial z}\right|_{z=0} = \left.\frac{\partial\Psi^I}{\partial z}\right|_{z=0} , \tag{10}$$

leads to the set of linear equations

$$K^{\perp}\delta_{i0} - A_i k_i^{\perp} = C_i k_i'^{\perp} + \sum_j C_j E_{j,i-j} , \tag{11}$$

where

$$E_{j,m} = \sum_n{}'' B_j(m,n)(k_j'^{\perp} + \vec{g}_{m,n}^{\perp}) .$$

Equations (9) and (10) can compactly be written in matrix notation

$$\begin{aligned} &(100..)^T + \vec{A} = \vec{\vec{P}}\,\vec{C} , \\ &(100..)^T - \vec{A} = \vec{\vec{Q}}\,\vec{C} , \end{aligned} \tag{12}$$

where

$$P_{ij} \equiv \delta_{ij} + D_{j,i-j}$$

and

$$Q_{ij} \equiv (k_j'^{\perp}\delta_{ij} + E_{j,i-j})/k_i^{\perp} .$$

Finally, we can solve these equations explicitly for the unknown column vectors $\vec{A}$ and $\vec{C}$,

$$\begin{pmatrix}\vec{A}\\ \vec{C}\end{pmatrix}=\begin{pmatrix}\vec{1} & -\vec{P}\\ \vec{1} & \vec{Q}\end{pmatrix}(-100\ldots100..)^T . \tag{13}$$

This equation is formally of infinite order. In practice, a good approximation can be obtained by limiting the number of beams to the finite number of propagating modes and a few evanescent waves. Under these conditions, the reflection and transmission coefficients are determined simply by inverting a matrix whose dimension is twice the number of beams considered.

III. EXACT SCATTERING DESCRIPTION

By adding and subtracting the matching equations (11), the column matrices A and C can be obtained separately so that

$$\begin{aligned}\vec{A}&=(\vec{P}-\vec{Q})(\vec{P}+\vec{Q})^{-1}(100..)^T ,\\ \vec{C}&=2(\vec{P}+\vec{Q})^{-1}(100..)^T .\end{aligned} \tag{14}$$

We focus our attention on the inverse of $(\vec{P}+\vec{Q})$. Let us define two diagonal and two off-diagonal matrices $\vec{P}_d$, $\vec{Q}_d$ and $\vec{P}_0$, $\vec{Q}_0$ such that

$$\begin{aligned}\vec{P}_d+\vec{P}_0&=\vec{P} ,\\ \vec{Q}_d+\vec{Q}_0&=\vec{Q} .\end{aligned} \tag{15}$$

Defining the off-diagonal matrix L as

$$\vec{L}=[(\vec{P}_d+\vec{Q}_d)^{-1}(\vec{P}_0+\vec{Q}_0)] \tag{16}$$

and substituting in $(P+Q)^{-1}$, we have

$$(\vec{P}+\vec{Q})^{-1}=\left(\sum_{N=0}^{\infty}(-\vec{L})^N\right)(\vec{P}_d+\vec{Q}_d)^{-1} . \tag{17}$$

The i,jth matrix element of $(\vec{P}+\vec{Q})^{-1}$ can thus be expressed as proportional to the sum of all possible products of the L_{ij},

$$\begin{aligned}&(P+Q)^{-1}{}_{ij}\\ &=[\delta_{ij}-L_{ij}+L_{ik}L_{kj}-L_{ik}L_{km}L_{mj}+\cdots](P_d+Q_d)^{-1}{}_{ij} ,\end{aligned} \tag{18}$$

where the summation convention over repeated indices is assumed. A discussion of the physical significance of the L_{ij} is given below.

From Eq. (14), the amplitude of the nth reflected beam can be obtained,

$$A_n=\sum_m(P-Q)_{nm}[(P+Q)^{-1}]_{m1} . \tag{19}$$

Defining $R_{ij}=(P-Q)_{ij}/(P_d+Q_d)_{ii}$ and substituting it and the expression for $(\vec{P}+\vec{Q})^{-1}$ into Eq. (17), the intensity of the specularly reflected (00) beam becomes

$$A_1=\sum_j R_{j1}\left(\sum_{N=0}^{\infty}(-\vec{L})^N\right)_{j1} . \tag{20a}$$

For the other (nonspecular) beams,

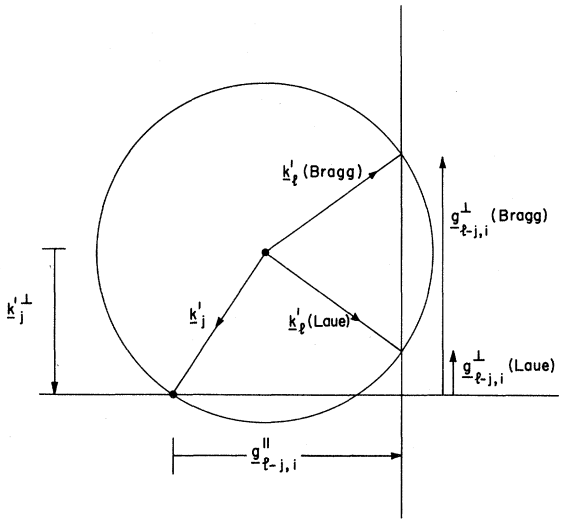

FIG. 2. Geometry of the scattering process in the limit of weak elastic scattering, when the constant energy surfaces are spherical. The scattered wave vectors for the reciprocal-lattice rod $g^{\parallel}_{i-j,i}$ are shown for both Bragg and Laue cases.

$$A_n=\sum_j R_{nj}\left(\sum_{N=0}^{\infty}(-\vec{L})^N\right)_{j1} \tag{20b}$$

These expressions are exact.

The physical significance of the expansion (20a) becomes apparent if we examine R_{ij} and L_{ij} in the limit of small elastic scattering. The exact expressions for R_{ij} and L_{ij} are

$$\left.\begin{matrix}L^{(+)}_{ij}\\ R^{(-)}_{ij}\end{matrix}\right\}=\frac{\sum_i[k^{\perp}_i\pm(k'^{\perp}_j+g^{\perp}_{i-j,i})]B_j(l-j,i)}{k^{\perp}_l+k'^{\perp}_l+\sum_i[k^{\perp}_i+(k'^{\perp}_i+g^{\perp}_{i-l,i})]B_i(l-l,i)} , \tag{21}$$

where the plus sign is taken for L_{ij} and the minus sign for R_{ij}. In the limit of small elastic scattering, the wave vectors inside and outside the crystal are equal, and the coefficients $B_j(\vec{g}_i)$ are large only when the Bragg condition is nearly satisfied, i.e.,

$$k'^{\perp}_j+g^{\perp}_{i-j,i}\simeq k'^{\perp}_i\simeq k^{\perp}_i$$

for a Laue (forward) scattering process, or

$$k'^{\perp}_j+g^{\perp}_{i-j,i}\simeq -k^{\perp}_i$$

for a Bragg (backward) scattering processes (see Fig. 2). Note that both $k'^{\perp}_j$ and $k^{\perp}_i$ have been defined to be positive quantities. At the Bragg condition, $B_j(\vec{g}_i)$ is of order unity, and hence

$L_{ij}\simeq 1$ for Laue reflection

$\simeq 0$ for Bragg reflection,

$R_{ij}\simeq 0$ for Laue reflection

$\simeq 1$ for Bragg reflection .

It must be emphasized that these results hold only

in the elastic limit as $V(r) \to 0$. For realistic potentials which include an imaginary component, the absolute magnitudes of L_{1j} and R_{1j} are always less than unity. The interpretation of the terms L_{1j} and R_{1j} as corresponding, respectively, to Laue and Bragg reflections from beam j to l enables us to interpret diagrammatically the expansion for the specularly reflected intensity;

$$A_1 = R_{11} + R_{11}\sum_{j\neq 1} L_{1j}L_{j1} - R_{11}\sum_{k\,p} L_{1k}L_{kp}L_{p1} + \cdots - \sum_{j\neq 1} R_{1j}L_{j1} + \sum_{j\,p} R_{1j}L_{jp}L_{p1} + \cdots . \quad (22)$$

Each term in this expansion may be represented by a diagram, and some examples are shown in Fig. 3. Figure 3(a) represents the term R_{11}, a Bragg reflection from the incoming beam to the specularly reflected beam. Figures 3(b) and 3(d) represent a double Laue scattering followed by a Bragg scattering; the former is the particular case when the second Laue scattering is from j to 1. The sum over all different beams in the second term of Eq. (22) accounts for all the independent ways of going from 1 (incoming) to 1 (outgoing) via a double Laue scattering. Figure 3(c) represents a typical Laue-Bragg process. Thus we see that the incident plane wave is scattered into all possible components of those Bloch waves which can be excited. For each component, the possibility of back scattering into the vacuum exists, thereby contributing to the specularly diffracted beam. A similar description holds for the nonspecular beams.

One advantage of viewing the scattering in this way is that it clarifies the relative importance of the three-dimensional potential and the two-dimensional matching process. On the one hand, each term in the expansion is a result of the matching conditions, yet each scattering term arising from the matching conditions contains as a factor the Bloch wave coefficients which are determined by the three-dimensional crystal potential.

IV. CONSISTENT SECOND-ORDER APPROXIMATION

The formalism to this point is exact. We now develop an approximation to the reflection amplitudes which is valid to second order in the expansion coefficients. The series [Eq. (22)] is first truncated to

$$A_1 \simeq R_{11} - \textstyle\sum_j R_{1j}L_{j1} . \quad (23a)$$

The intensity of the 00 (specular) beam is given in this approximation by

$$I_{00} = |A_1|^2 = |R_{11} - \textstyle\sum_j R_{1j}L_{j1}|^2 . \quad (23b)$$

A consistent expression for I_{00} up to second order requires that the expansion coefficients in R_{1j} and L_{j1} $(j \neq 1)$ be calculated to *first order* and those in R_{11} be calculated to *second order*.

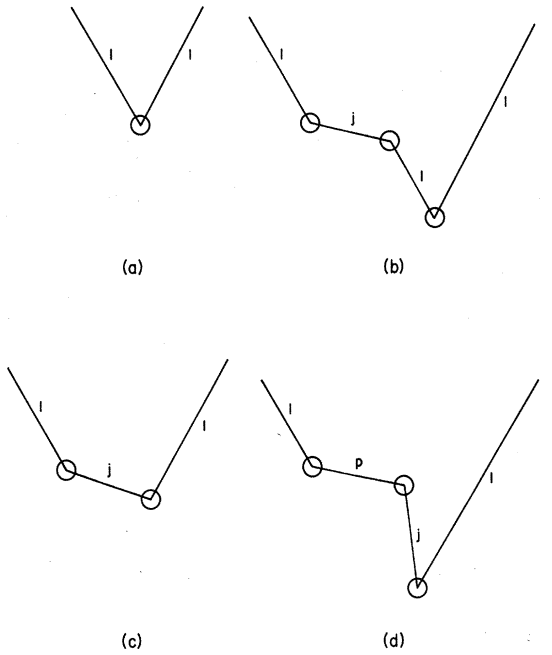

FIG. 3. Diagrammatical representation of terms in the exact scattering expansion for the specularly reflected beam [Eq. (22)].

A. First-Order Terms

To the lowest nontrivial order,

$$k_j'^{\perp} = (E + \langle k_j'|V|k_j'\rangle - |\vec{K}^{\parallel} + \vec{g}_j^{\parallel}|^2)^{1/2} \quad (24a)$$

and

$$B_j(\vec{g}_l) = \frac{\langle \vec{k}_j' + \vec{g}_l | V | \vec{k}_j' \rangle}{k_j'^2 - |\vec{k}_j' + \vec{g}_l|^2} . \quad (24b)$$

In Eq. (24a), the diagonal element $\langle k_j'|V|k_j'\rangle = W - \Gamma(k_j')$, where W is the work function and $\Gamma(k_j') = \Gamma_1 + i\Gamma_2$ is a complex term which is calculated self-consistently with k_j'. The imaginary part of this term accounts for the inelastic electron-electron scattering and its effect is to add an imaginary part of $k_j'^{\perp}$ of the order of $\Gamma_2/2E^{1/2}$.

B. Second-Order Terms

Inspection of R_{11} reveals that the only coefficients to be evaluated to second order are $B_1(1,i)$, where the index i runs along the 00 rod. These are given by standard second-order theory[31]

$$B_1(1,i)[2] = B_1(1,i)[1]\left[1 + \sum_{\substack{\vec{g}_l \neq \vec{g}_i^{\perp} \\ \vec{g}_l \neq 0}} \frac{\langle \vec{k}_1' + \vec{g}_i^{\perp} | V | \vec{k}_1' + \vec{g}_l \rangle}{\langle \vec{k}_1' + \vec{g}_i^{\perp} | V | \vec{k}_1' \rangle} B_1(\vec{g}_l)[1] + \left(\frac{\langle \vec{k}_1' + \vec{g}_i^{\perp} | V | \vec{k}_1' + \vec{g}_i^{\perp} \rangle - \langle \vec{k}_1' | V | \vec{k}_1' \rangle}{\langle \vec{k}_1' + \vec{g}_i^{\perp} | V | \vec{k}_1' \rangle}\right) B_1(1,i)[1]\right], \quad (25)$$

where $B_1(1,i)[2]$ is the coefficient calculated to second order and the $B_1(\vec{g}_l)[1]$ are the coefficients calculated to first order from Eq. (24b).

C. Justification of Approximation

Perturbation theory is usually considered valid if the coefficients $B_j(\vec{g}_l)[1]$ are much less than unity. For k_j' real, $B_j(\vec{g}_l)$ exhibits a singularity at the Bragg condition

$$k_j'^2 = |\vec{k}_j' + \vec{g}_l|^2 .$$

If k_j' is complex, however, with imaginary part $\mathrm{Im}(k_j')$, it is easy to show that

$$B_j(\vec{g}_l) = \frac{\langle \vec{k}_j' + \vec{g}_l | V | \vec{k}_j' \rangle}{2\cos^2\theta\, \Delta E - 2ig_j^{\perp}\mathrm{Im}(k_j')} , \tag{26}$$

where ΔE is the energy measured relative to the free-electron resonance energy

$$E_{\mathrm{res}} = g_j^2/(2\cos\theta)^2$$

and θ is the angle between $\vec{k}_j'$ and $\vec{g}_j$. A nonvanishing $\mathrm{Im}(k_j')$ removes the singularity in $B_j(\vec{g}_l)$, the maximum value of $|B_j(\vec{g}_l)|$ now being

$$\tfrac{1}{2}\langle \vec{k}_j'^{\perp} + \vec{g}_l | V | \vec{k}_j'^{\perp} \rangle / g_j^{\perp}\mathrm{Im}(k_j') . \tag{27}$$

Perturbation theory should be appropriate when this quantity is much smaller than unity. This is true for most of the coefficients in a typical LEED calculation.

An important exception occurs for $B_j(\vec{g}_l)$ corresponding to reciprocal-lattice points in the plane of the surface, i.e., those for which $g_j^{\perp}$ is identically zero. These include vectors which connect plane waves degenerate by symmetry. In the calculation reported here, the incident wave vector lies in the xz plane and rotates about the $[11\bar{2}0]$ symmetry direction. The reciprocal lattice viewed normal to the surface is shown in Fig. 4. The finite angle of incidence breaks the rotational symmetry about the z axis. The reflection symmetry across the xz plane persists, however, and the pairs of waves (4, 5), (6, 7), (8, 9), etc., are degenerate. Degenerate perturbation theory must be used and we proceed by solving exactly the related 2×2 secular equations and substituting the correct linear combination of the two plane waves in the formalism.

D. Occurrence of Secondary Peaks

The occurrence of secondary peaks is a natural consequence of any treatment which includes dynamical effects. In the present formalism, secondary structure will arise if either of the terms R_{11} or $R_{1j}L_{j1}$ is large. In the former case, secondary effects may appear on the shoulders of the Bragg peak due to an increase in $B_1(1,i)$. From Eq. (25), we see that the second term is a maximum for the simultaneous occurrence of a Bragg reflection in the specular beam and another Bragg or Laue reflection in a different beam. In the latter case, when a Bragg and Laue reflection occur together along the same reciprocal-lattice rod (m), the relevant term is $R_{1m}L_{m1}$, both factors of which are large. The effect on the specular beam is therefore a maximum. Shifts in the propagation vectors by a large inner potential and/or band-structure effects relax the necessary condition for the simultaneous excitation and secondary peaks will be large for *either* a Bragg or Laue reflection in a nonspecular beam. This condition is identical to that derived by McRae[7] for the general occurrence of secondary peaks.

V. POTENTIAL

To apply the formalism in a specific case, it is necessary to know, in detail, the momentum-dependent Fourier components of the scattering potential. These determine the coefficients of the Bloch states $B_j(g_l)$ of the wave function inside the crystal and hence the elements of the matching matrices. In this paper, we calculate intensity-voltage curves for beryllium, for which detailed experimental results are available. For the theorist, beryllium

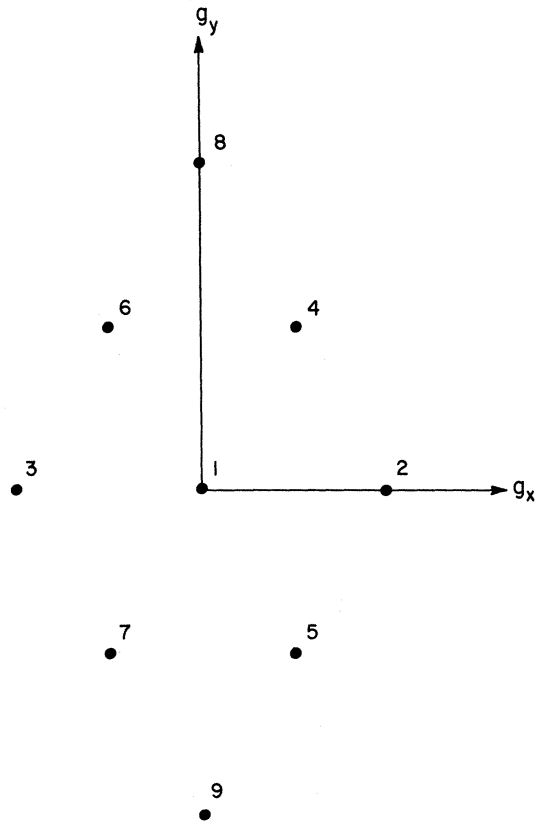

FIG. 4. Parallel components of the bulk crystal reciprocal-lattice vectors used in the present calculation. For rotation of the incident beam about the y axis, the vectors (4, 5), (6, 7), and (8, 9) are degenerate in pairs. The numerical values of the vectors are given in Table II.

has distinct advantages over other materials which have been studied by LEED. (a) The wave function of the 1s core electrons is well described by a simple spherically symmetrical function. Integrals arising in the Fourier transform of the pseudopotential can be evaluated in closed form and effect a large computational saving. (b) Recent band-structure calculations and Fermi-surface measurements provide an independent check of the calculated pseudopotential. (c) The Debye temperature of beryllium is 1160 °K [32] and, since the cleavage and data collection were made at liquid-nitrogen temperatures, thermal effects of Debye-Waller type should be considerably less than for most other materials. Each of these points will be discussed in detail below. We now consider the contributions to the effective one-electron potential in beryllium and calculate the matrix elements, diagonal and off diagonal, with respect to plane-wave states. In some ways, the discussion parallels that of Harrison. [33]

We make the customary assumption that the crystal may be regarded as a superposition of localized atomic potentials

$$V(\vec{r}) = \sum_\tau V_a(\vec{r} - \tau) ,$$

where τ denotes the atomic positions. In this case, scattering matrix elements between plane-wave states can be written as the product of the Fourier transform of the atomiclike potential (or pseudopotential) and the structure factor $S(g)$, where

$$S(\vec{g}) = (1/N)\sum_\tau e^{-i(\vec{g}\cdot\vec{\tau})} , \tag{28}$$

where N is the number of atoms, and $\vec{g}$ is the scattering vector. The structure factor clearly depends on the choice of origin in coordinate space and on the number of atoms in the unit cell. The primary contributions to the one-electron potential are the ion-core potential V_H, the core-valence exchange V_x, the orthogonalization term V_R, which converts the potential into a pseudopotential, and V_{ce}, the potential due to the conduction electrons.

A. Off-Diagonal Terms

1. *Core Potential Term*

A dominant term is the core potential due to the nuclear charge plus core electrons. If the 1s core state wave function is written $\psi_c(r)$, then this term, the Hartree potential, is

$$V_H(\vec{r}) = 2\left(\frac{-4}{r} + 2\int \frac{d^3r' \, |\psi_c(r')|^2}{|r - r'|}\right). \tag{29}$$

The work of Holöien [34] shows that a core wave function of hydrogenic type

$$\psi_c(r) = (\alpha^3/\pi)^{1/2} e^{-\alpha r} , \tag{30}$$

with α determined variationally to be $3.51 a_0^{-1}$, gives a ground-state energy close to the Hartree-Fock energy. If we adopt this analytic form, the Fourier transform of the Hartree potential may be evaluated directly. [35] An alternative analytic wave function has been developed for beryllium by Shull and Löwdin, [36] which takes into account core-correlation effects. The Fourier transform of the resultant potential has been tabulated, [37] and we have used these values for $R(g)$, although the difference between the two is small:

$$\langle \vec{k} | V_H | \vec{k} + \vec{g} \rangle = -\frac{4\pi}{\Omega_0}\left(\frac{2R(\vec{g})}{g^2}\right) . \tag{31}$$

2. *Evaluation of Core-Plane-Wave Exchange*

In evaluating core-plane-wave exchange, a number of possible approaches may be taken. The first is the evaluation of matrix elements of the exact nonlocal exchange operator arising from the Hartree-Fock equations:

$$V_x \phi(r) = -\int \frac{d^3r'}{|r - r'|} \psi_c^*(r')\psi_c(r)\phi(r') . \tag{32}$$

For plane-wave states, it is possible to evaluate this analytically, but the final expression is extremely cumbersome and approximations to it [35] are not applicable due to the large range of incident plane-wave energies. Moreover, it has become apparent from work on band-structure calculations and on many-body systems that the exclusion of correlation effects in the Hartree-Fock method leads to errors substantially greater than approximate methods based on the local density of both spins (e.g., Slater [38]). Such approximations have been discussed recently in some detail. [39, 40] In atomic calculations, we are generally interested in exchange effects between orthogonal orbitals. In the present case, the plane wave and the hydrogenic core state are not orthogonal, and we have adopted an approximation which takes this into account. [41] Although related to the local-density approximations, this exchange potential depends explicitly on the wave vector of the plane wave, and its Fourier transform depends on both $\vec{k}$ and $\vec{g}$, as in the case of a nonlocal potential,

$$\langle \vec{k}_1 + \vec{g}_1 | V_x | \vec{k}_2 + \vec{g}_2 \rangle = -\frac{4\pi}{\Omega_0}\left(\frac{27.8102\,\alpha^{14/3}}{(\alpha^2 + |\vec{k}_2 + \vec{g}_2|^2)^{4/3}\left[\frac{16}{9}\alpha^2 + |\vec{k}_2 + \vec{g}_2 - \frac{5}{3}(\vec{k}_1 + \vec{g}_1)|^2\right]^2}\right) . \tag{33}$$

To preserve Hermiticity of the potential, this matrix element is replaced in our calculation by half the the sum of itself plus its Hermitian conjugate. In the limit of very high-energy plane waves this con-

tribution to the potential vanishes, and at low energies it is comparable to the Slater approximation. A discussion of this and other exchange approximations is given in Appendix A.

3. *Contribution to Conduction-Electron Potential*

A substantial simplification in assessing the contribution to the potential of the conduction electrons results from the work of Loucks and Cutler.[42] By evaluating the self-consistent one-electron potential using the orthogonalized-plane-wave (OPW) formalism, they found that this contribution to the potential is essentially the same as that given by assuming a uniform distribution of electrons. This result reflects, of course, the small fraction of the atomic volume which is occupied by the core. The assumption of a uniform distribution of conduction electrons, which we adopt here, means that its effect will be mainly on the diagonal terms. The conduction electrons give rise, however, to screening of the off-diagonal Fourier components.

For a local potential (i.e., one whose Fourier transform depends only on the momentum transfer $\vec{g}$), the screening is described by dividing $\langle \vec{k}| V |\vec{k}+\vec{g}\rangle$ by the Hartree dielectric function. The potential we develop is dependent on both $\vec{k}$ and $\vec{g}$, and the screening should reflect this, as discussed by Harrison[33] and by Animalu,[43] amongst others. The numerical calculations of Animalu show, however, that for $\vec{k}=\vec{k}_F$, local and nonlocal screening lead to essentially the same matrix elements for Li, Al, and Pb. For higher $\vec{k}$ values, the momentum-dependent terms in the potential are smaller, and the errors due to the local-screening approximation should be correspondingly less. For these reasons, in addition to its simplicity of form, we use Hartree screening.

The remaining term in the potential is the orthogonalization term V_R which converts the potential into a pseudopotential, with eigenfunctions for which plane waves are an appropriate basis. A recent examination of the pseudopotential formalism made by Pendry[44] in the light of an analysis of Weinberg,[45] suggested as the form most appropriate at all energies

$$V_R = -E_c |c\rangle\langle c| \ , \tag{34}$$

where E_c is the energy corresponding to the core-state wave function $|c\rangle$. It is a member of the Austin, Heine, and Sham[46] family of pseudopotentials, and is Hermitian. In our calculations the overlap integrals can be evaluated in closed form and the final result is

$$\langle \vec{k}| V_R |\vec{k}+\vec{g}\rangle = \frac{4\pi}{\Omega_0}\left(\frac{16\,E_c\,\alpha^5}{(\alpha^2+k^2)^2\,(\alpha^2+|\vec{k}+\vec{g}|^2)^2}\right). \tag{35a}$$

As described above, the final pseudopotential is screened by the Hartree dielectric function, and may therefore be written

$$\langle \vec{k}| V |\vec{k}+\vec{g}\rangle = [\,V_H(\vec{g}) + V_x(\vec{k},\vec{g}) + V_R(\vec{k},\vec{g})]/\epsilon(\vec{g}) \ , \tag{35b}$$

where

$$\epsilon(\vec{g}) = 1 + (2\pi k_F \eta^2)^{-1}\left[1 + \frac{1-\eta^2}{2\eta}\ln\left(\frac{1-\eta}{1+\eta}\right)\right]$$

and

$$\eta = g/2k_F \ .$$

An independent check of the calculated matrix elements for beryllium is provided by recent de Haas–van Alphen measurements of the Fermi surface.[47] These workers used a pseudopotential of the OPW form

$$\langle \vec{k}| V_{ps} |\vec{k}+\vec{g}\rangle = V'(\vec{g}) + (E-E_c)\langle \vec{k}|c\rangle\langle c|\vec{k}+\vec{g}\rangle \tag{36}$$

and used as adjustable parameters E_c and the Fourier components $V'(\vec{g})$ for the four reciprocal-lattice vectors near the Fermi sphere. Since they have not screened their potential, direct comparison of the local parts $V'(\vec{g})$ with the present work is not possible. However, matrix elements for initial state $|\vec{k}\rangle$ and final states $|\vec{k}+\vec{g}\rangle$ both lying on the Fermi sphere should be similar. We have evaluated these matrix elements for the potential described above and have adjusted the core-state energy E_c in Eq. (34) so that the form factors for $\vec{g} = 10\bar{1}0$, 0002, $10\bar{1}1$, $10\bar{1}2$ are the best least-squares fit to the Fermi-surface results. In fact the core shift is small, the fitted value being 9.305 Ry and the Hartree-Fock value 8.698 Ry.[47] The matrix elements, together with those calculated from the model potential of Animalu and Heine[48] are shown in Table I.

B. Diagonal Matrix Elements

In evaluating the diagonal matrix elements and, in particular, corrections to the energy due to the Coulomb interactions between conduction electrons, a number of approximations are necessary. Of prime importance in the present calculation is the inclusion of inelastic effects via the self-energy or the exchange-correlation potential of the interacting system. At the present time, the only calculations of this quantity have been carried out for the translationally invariant electron gas in which the conduction electrons interact in the presence of a uniform positive background. For this system, calculations have recently been performed for various electron gas densities by Lundqvist[49] and we have adopted his results, as discussed below.

The use of the electron gas approximation for the conduction electrons requires justification but for a metal like beryllium, the approximation seems to be a very good one. As discussed above, Loucks and Cutler[42] showed that the conduction electron

potential in beryllium is very close to the potential in a uniform distribution of electrons.

The effects of the nucleus, the core electrons and core-plane-waves exchange on the energy, are found by evaluating the appropriate diagonal matrix elements. Using the analytic form [Eq. (30)] for the core potential and the ($\vec{k}$-dependent) diagonal matrix element of the exchange potential, this can readily be carried out. The contributions of screening and orthogonalization to the average potential are neglected since the main consequences are to redistribute the electronic charge but not to change its average value. As pointed out by Harrison,[33] the average potential will not be greatly affected. Effects of the "orthogonalization hole" are also neglected. Calculations using the approximate formula of Harrison[33]

$$Z^*/Z = 1 + \langle \vec{k} \mid c \rangle \langle c \mid \vec{k} \rangle$$

suggest an energy-dependent renormalization of the core charge of at most 6%. To show that the effect on the average potential energy of the above contributions is adequately represented by the uniform positive background, we have calculated the energy of a uniform distribution over the atomic volume of a positive charge equal to the valence. The small difference between the energies due to the actual core and the uniform positive distribution has been included in the calculation.

The single-particle properties of an interacting electron gas are conveniently described by a self-energy $\Sigma(k, \epsilon)$ which is a complex potential energy term. The real part causes a shift in the single-particle energy, the imaginary part leads to broadening of the state due to the Coulomb interactions present. To evaluate the self-energy, Lundqvist[49] expanded in terms of the deviation of the excitation energy $(\epsilon - \mu)$ from the free-particle value $(k^2 - k_F^2)$. To first order,

$$\Sigma(k, \epsilon) = \epsilon_0 + [\Sigma(k, k^2) - \epsilon_0] \left(1 - \frac{\partial \Sigma}{\partial \omega}(k, k^2)\right)^{-1}, \tag{37}$$

where $\epsilon_0 = \Sigma(k_F, k_F^2)$. Lundqvist has evaluated all terms in this expansion, using the random-phase approximation (RPA), and has graphed the results.

TABLE I. Beryllium form factors (matrix elements $\langle \vec{k} | V | \vec{k} + \vec{g} \rangle$ for which initial and final states both lie on the Fermi sphere). The results are normalized to the volume of the unit cell.

g	TEGS (Ref. 47)	This calculation	AH (Ref. 48)
$10\bar{1}0$	0.0571	0.0485	0.0334
0002	0.0889	0.0796	0.0470
$10\bar{1}1$	0.0981	0.0896	0.0479
$10\bar{1}2$	0.0976	0.1235	0.0318

In the present calculation, the resultant numerical values for $\Sigma(k, \epsilon)$ give the contribution $\Gamma_1(k_j') + i\Gamma_2'(k_j')$ to the diagonal matrix elements $\langle k_j' | V | k_j' \rangle$ of Eq. (24a).

C. Thermal Effects

The effect of lattice vibrations on electron and x-ray scattering is usually[50] included by multiplying each matrix element $\langle \vec{k} \mid V \mid \vec{k} + \vec{g} \rangle$ by $e^{-M(g)}$, where M is the Debye Waller factor

$$M = \tfrac{1}{2} \sum_q | \vec{g} \cdot \vec{U}_q |^2 . \tag{38}$$

Here $\vec{g}$ is the scattering vector and $\vec{U}_q$ the amplitude of the qth lattice mode. The loss in intensity in the elastic-scattered component due to the Debye-Waller factor appears in the form of thermal diffuse scattering (TDS) corresponding to inelastic-scattering processes involving one or more phonons. Discussions of TDS in the literature are generally restricted to the dominant single-phonon term which, depending on the temperature and crystal involved, can be a significant factor in the scattering process. In particular, if the TDS component is large and if the experimental arrangement is such that TDS is not collected along with the elastic scattering, the Debye-Waller factor must be included in the theory. On the other hand, if TDS occurs primarily in the neighborhood of the reciprocal-lattice rod and the aperture of the collector is large enough to include most of the TDS, it is more appropriate not to include the Debye-Waller factor at all. Of course, conditions intermediate between these extremes would be quite difficult to handle.

The angular dependence of TDS has been discussed in the high-temperature limit by Huber[51] and the prediction that the intensity varies inversely with the distance from the nearest reciprocal-lattice rod has been verified experimentally.[52] In the case of low temperatures, we show in Appendix B that the TDS is much more evenly distributed throughout the zone. We therefore include the Debye-Waller factor in our scattering matrix elements. In the zero-temperature limit appropriate for the beryllium data of Baker

$$M = \tfrac{3}{4} (m/m_b) | \vec{g} |^2 / k\Theta_D , \tag{39}$$

where m is the electron mass, m_b the atomic mass, and Θ_D is the Debye temperature of beryllium (1160 °K).

D. Discussion

The form factors of the potential, as a function of the scattering vector $\vec{g}$ at various energies, are shown in Fig. 5. An important feature of these curves is the angular dependence of the scattering matrix elements for a given energy. For most energies, forward scattering is considerably stronger

than backward scattering, and this may be regarded as a general characteristic of the LEED scattering process. It therefore seems unlikely that any isotopic scattering model, such as one using purely s-wave phase shifts, will lead to quantitatively correct reflectivities.

The evaluation of the potential matrix elements has involved a number of approximations. In particular, inelastic effects of a periodic nature are neglected, so that the off-diagonal elements are purely real. Imaginary contributions may come from core excitation processes, or from periodic effects in the electron gas. The former may occur near 100 eV in beryllium and are neglected here, while recent work[53] suggests that the contribution of the latter should be negligible in a small-core material such as beryllium.

Inelastic terms affect, therefore, only the diagonal matrix elements in the potential. Additional support for this approximation is provided by the work of Bassani, Robinson, Goodman, and Schrieffer.[54] Their analysis, in which many-body effects are included using an orthogonalized plane wave, rather than a plane-wave basis, indicates that the best low-order description of many-body effects in real metals results from the addition of the homogeneous electron gas self-energy to the potential used in the band calculation. A recent discussion of this problem has been given by Hedin and Lundqvist,[55] with similar conclusions.

VI. RESULTS AND DISCUSSION

Before presenting the results and a comparison with experiment, a further discussion of the mechanics of the calculation is necessary. In particular (i) the matching plane is taken half-way between atoms by a suitable choice of the unit-cell basis vectors in the calculation of the structure factor $S(\vec{g})$ [see Eq. (28)]. This is a common choice and is particularly appropriate in a pseudopotential approach since the pseudo-wave-function and the real wave function are very similar midway between atoms. (ii) The beams included in the calculation are the nine shown in Fig. 4, and are given in Table II. This means that we include nine distinct reciprocal-lattice rods $\vec{g}_i^{\,\parallel}$ and that the sum in Eq. (23) is over eight terms. Along each rod, ten perpendicular components $\vec{g}_{i,j}^{\,\perp}$ are taken, giving a total of 90 plane waves in terms of which the relevant Bloch waves are expanded. As a test of the adequacy of nine beams, we have increased the number to 18 and noted little change in the calculated diffracted intensities. (iii) The calculations are performed from 0 to 200-eV incident energy at angles of incidence from 0° to 18° in 2° intervals. The incident beam lies in the zx plane. (iv) Finally, we set the real part of the diagonal term $\langle k_j' | V | k_j' \rangle$ equal to zero and compensate the resulting shift in the intensity-voltage curves by adding this term to the voltage. The justification of this procedure lies in an attempt to eliminate the back reflection produced by the large discontinuity in the potential which is an unavoidable feature of the wave-matching approach. The real situation at the surface is somewhat different and modification of the approach is in order. In particular, the potential falls off to zero rather smoothly over a distance of a few angstroms, resulting in a decreased step reflection and a reduced perturbation in the reflected beams. Setting the real part of the diagonal matrix element equal to zero effectively eliminates this spurious reflection. A more rigorous solution is to describe the physical space of the problem as three regions—bulk, surface, and vacuum—and to perform the matching calculations at the two interfaces. Such calculations are in progress and will be reported at a later time.

In Figs. 6 and 7 the results of the calculation[56] are compared with the experimental work of Baker.[29] We note several marked similarities. A Bragg peak at 180 eV becomes less intense as θ increases; a very prominent peak at approximately 90 eV appears near $\theta = 12°$; a weak peak occurs at low energies (~ 30 eV) and both the first Bragg peak and the peak near 150 eV split as θ increases. The calculated reflectivities in the first peak are typically 6% and in the highest-energy peak shown they are the order of 0.05%. A precise comparison of these reflectivities with experiment is difficult to make, due to some experimental uncertainties.[29] However, the reflectivity range observed for the same peaks is 4–0.1%, so that there is at least order of magnitude agreement.

The calculation proceeds very rapidly with an I-V curve of 100 points, requiring only 1 min on an IBM 360-67 computer. The speed of computation enables us to examine the convergence of the second-order calculation and the sensitivity of the intensity curves to changes in the parameters in the potential. If we evaluate the reflectivity using only the first term (R_{11}) in Eq. (22), but evaluate this term exactly rather than to second order, we find

TABLE II. Parallel components (g_x, g_y) of bulk crystal reciprocal-lattice vectors shown in Fig. 4.

Vector	g_x	g_y
(1)	0	0
(2)	1.69122	0
(3)	−1.69122	0
(4)	0.84561	1.46465
(5)	0.84561	−1.46465
(6)	−0.84561	1.46465
(7)	−0.84561	−1.46465
(8)	0	2.92930
(9)	0	−2.92930

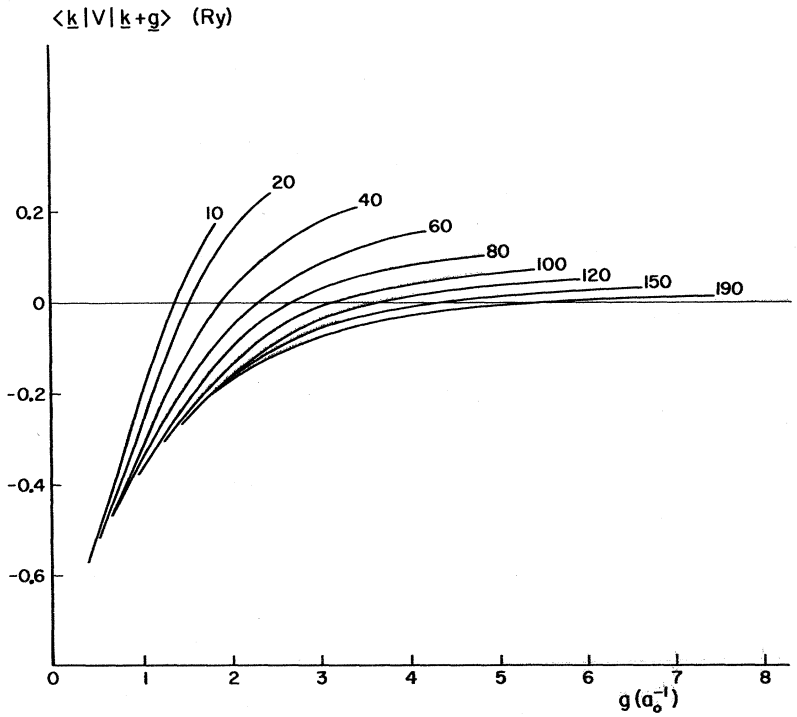

FIG. 5. Each curve is labeled by an energy E in electron volts. The ordinate is the matrix element $\langle \vec{k} | V | \vec{k}+\vec{g} \rangle$ (form factor) for which the abscissa $\vec{g}$ is chosen so that both $\vec{k}$ and $\vec{k}+\vec{g}$ lie on the constant energy surface E.

that the results are substantially the same. Although higher-order corrections may be evaluated in a straightforward though tedious manner, this result suggests that the second-order calculation is a good approximation to the exact-matching procedure.

The sensitivity of the results to changes in the real and imaginary parts of the scattering potential has been examined in the following ways: (i) Different approximations for the core-plane-wave exchange have been used. In addition to the modified Slater exchange discussed above, we have used the Slater approximation and have set V_x equal to zero. We have run these calculations with the core-state

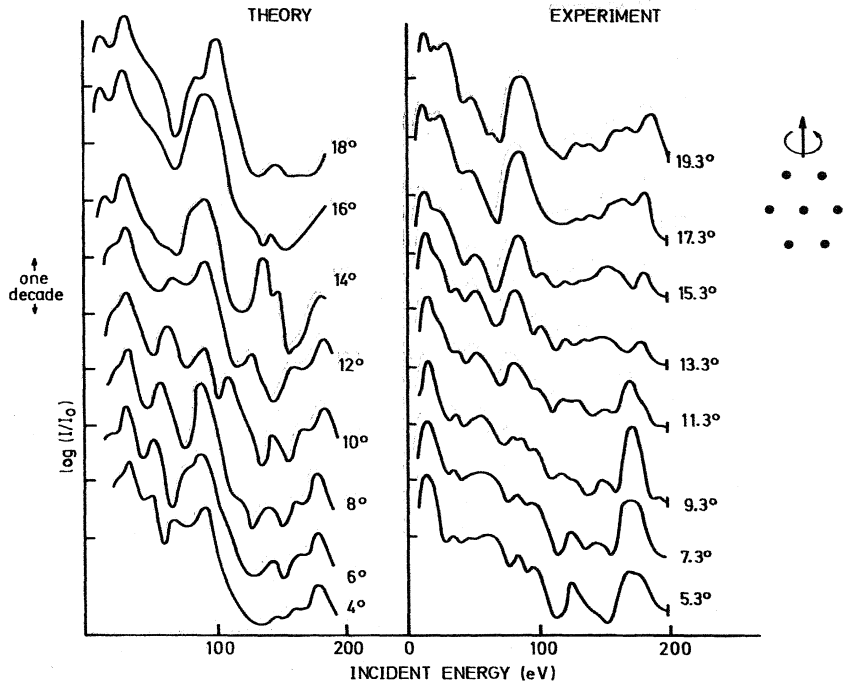

FIG. 6. Theoretical and experimental intensity-voltage curves for the (0001) face of beryllium with rotation about $(11\bar{2}0)$. Angles of incidence are as marked, incident energies are in electron volts, and intensities are log normalized. One decade in intensity is shown at the left.

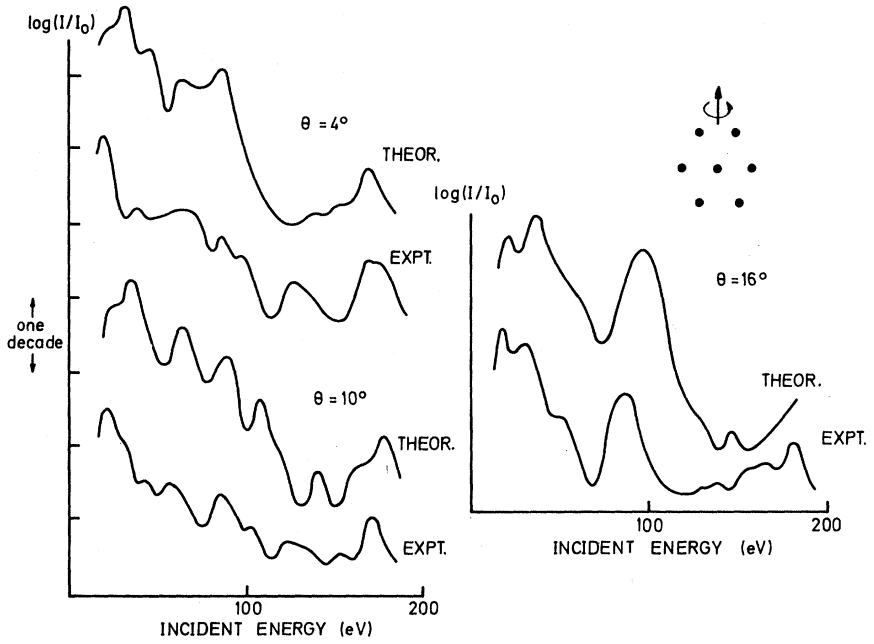

FIG. 7. Direct comparison of theory and experiment for $\theta = 4°$, 10°, and 16°.

energy set equal to the free-atom value and also adjusted, in the respective cases, to give the best least-squares fit to the experimental matrix elements. (ii) We have run the calculation using the OPW form of the pseudopotential. Although this form is explicitly energy dependent, it is no complication in the present approach in which the eigenvalue is the momentum. (iii) The imaginary part of the self-energy has been set equal to a number of constant values. (iv) As discussed above, the change in scattering matrix elements due to the Debye-Waller factor and the resultant change in diffracted intensity should be small in beryllium. This has been tested.

The results show that some features of the calculated I-V curves are rather insensitive to the above changes. The reflectivity is much higher at energies below the threshold for plasmon creation and falls as the imaginary part of the scattering potential increases. This is a general feature of the results, as is the relative insensitivity of the peak positions and peak widths. The *absolute* intensities vary significantly, however, and this confirms the earlier observation[22] that this quantity should be a much more sensitive probe of the scattering potential than the peak width. The greatest changes in reflectivity are observed when the OPW matrix elements [see the form of Eq. (36)] replace those of the pseudopotential described above. For incident energies near 200 eV, the absolute intensity is increased significantly.

This emphasizes the importance of an appropriate choice of pseudopotential for use in LEED calculations. Near the Fermi energy, the form factors of the two potentials are virtually identical and for transport phenomena will give very similar results. At very high energies the orthogonalization term vanishes and the potentials are identical. For LEED energies, however, the pseudopotentials have quite different matrix elements, particularly for back scattering, and LEED provides, therefore, a good test of the Pendry criteria.

The present calculations demonstrate that experimental features may be reproduced over a wide range of incident angles and energies. The sensitivity of the reflectivities to the scattering potential and, in particular, to the shape of the barrier at the surface, encourages the hope that careful absolute intensity measurements will lead to a much improved knowledge of the surface potential.

ACKNOWLEDGMENTS

Dr. J. M. Baker has very kindly provided us with experimental data prior to publication. We thank him, and also Dr. N. W. Ashcroft, Dr. J. M. Blakely, Dr. F. Jona, Dr. C. Y. Li, Dr. T. N. Rhodin, and Dr. J. W. Wilkins for helpful discussions.

APPENDIX A: DISCUSSION OF EXCHANGE APPROXIMATION

The simplified treatment of the exchange term[57] [Eq. (31)] given by Slater[38] has proved very useful in atomic structure and energy band calculations. In a free-electron gas, the exchange potential is

$$V_x^F = -4\left(\frac{3}{8\pi}\rho\right)^{1/3}\left(1+\frac{1-\alpha^2}{2\alpha}\ln\left|\frac{1+\alpha}{1-\alpha}\right|\right). \quad \text{(A1)}$$

In this equation, ρ is the electron density and $\alpha = k/k_F$. Slater averaged this expression over occupied states ($k < k_F$) and obtained the well-known result

$$V_x^S = -6\,[(3/8\pi)\,\rho(r)]^{1/3}\,, \tag{A2}$$

where $\rho(r)$ is now the local density of the core electrons. Evaluating V_x^F at $k = k_F$ leads to the result of Gáspár[58] and of Kohn and Sham,[59]

$$V_x^{KSG} = -4\,[(3/8\pi)\,\rho(r)]^{1/3}\,. \tag{A3}$$

A number of modifications of these approximations have been suggested,[39,60,61] and recently compared.[40] The criteria for success are taken to be the closeness of the ground-state energy and the radial charge density of the *atom* to the Hartree-Fock values. For practical calculations, Slater *et al.*[40] concluded that Eq. (A2) was the best choice.

A more sensitive test for energy band purposes would be to evaluate the Fourier components of the approximate potential and compare with the exact results. This may be done for hydrogenic wave functions of the type considered here [Eq. (30)] and was carried out by Meyer and Young.[35] The results show significant discrepancies. These differences have their origin in the assumptions of the Slater approximation, which we now examine for the specific case of core-valence exchange. The Slater argument, which holds true for the *total* exchange operator, does not apply to core terms alone. This is due to the nonlinearity of the $\rho^{1/3}$ approximation, i.e., $(\rho_v+\rho_c)^{1/3} \neq (\rho_v^{1/3}+\rho_c^{1/3})$, where ρ_v and ρ_c are the charge densities of valence and core electrons. The consequences of nonlinearity are clarified by a calculation of a typical core-valence exchange matrix element using the *physical* arguments of Slater in his justification of the $\rho^{1/3}$ approximation. The results suggest a new momentum-dependent exchange operator, whose matrix elements more closely approximate the actual exchange terms. The Schrödinger equation for the one-electron valence states in the crystal ψ_v is

$$[-\nabla^2 + (V_v + V_{xv}) + (V_c + V_{xc})]\,\psi_v = E_v\psi_v\,, \tag{A4}$$

where V_v, V_c, and V_{xv}, V_{xc} are, respectively, Coulomb potentials and exchange operators for the valence and core electrons. Standard many-body techniques are usually invoked to discuss $(V_v + V_{xv})$, and V_c follows from a knowledge of the core wave functions. The linearity of the exact exchange operator allows its separation into valence and core terms. The latter, which is often approximated by a $\rho^{1/3}$ term, is

$$\langle\psi_v \,|\, V_{xc} \,|\, \psi_v\rangle = \sum_c \int \psi_v^*(1)\psi_c(1)(1/r_{12})\psi_v(2)\psi_c^*(2)\,dv_1\,dv_2\,, \tag{A5}$$

where the sum is over all core orbitals with spin parallel to the valence state. Following Slater, we write

$$\langle\psi_v \,|\, V_{xc} \,|\, \psi_v\rangle = \left\langle \psi_v \,\middle|\, \left\{ \sum_c \frac{\psi_v^*(1)\psi_c(1)\psi_v(2)\psi_c^*(2)\,dv_2}{r_{12}\psi_v^*(1)\,\psi_v(1)} \right\} \,\middle|\, \psi_v \right\rangle = \left\langle \psi_v \,\middle|\, \left\{ \int \frac{\rho(1,2)}{r_{12}}\,dv_2 \right\} \,\middle|\, \psi_v \right\rangle . \tag{A6}$$

The expression in the braces may be interpreted as a potential at r_1 due to a charge distribution $\rho(1, 2)$, where

$$\rho(1,\,2) = \sum_c \frac{\psi_v^*(1)\,\psi_c(1)\,\psi_v(2)\,\psi_c^*(2)}{\psi_v^*(1)\,\psi_v(1)}\,. \tag{A7}$$

We wish to approximate this nonlocal charge distribution by one more amenable to calculation. The charge density at 1 is

$$\rho(1,\,1) = \textstyle\sum_c \psi_c^*(1)\,\psi_c(1)\,,$$

which is just the charge density of core electrons with parallel spin at point 1. The total charge is

$$\rho(1) = \int \rho(1,2)\,dv_2 = \sum_c S_c\,\frac{\psi_v^*(1)\,\psi_c(1)}{\psi_v^*(1)\,\psi_v(1)}\,,$$

where

$$S_c = \int \psi_c^*(2)\,\psi_v(2)\,dv_2 \tag{A8}$$

is the overlap integral between ψ_v and ψ_c. Differences between this formulation and the original argument of Slater are now apparent. In atoms, one is normally interested in orthogonal orbitals for which case

$$\rho(1) = 1, \quad \rho(1,1) = \sum_{c_{11}} \psi_c^*(1)\,\psi_c(1)\,,$$

where all orbitals [including $\psi_v(1)$] are included in the summation.

In our treatment, we exclude from the summation the orbital $\psi_v(1)$, since this term is always cancelled by the self-Coulomb term. Extending Slater's physical arguments, the exchange integral can be regarded as the expectation value of the potential due to an electron charge density whose value at point (1) equals the charge density of parallel spin there, and whose total charge is

$$\rho(1) = \sum_c S_c\,\frac{\psi_v^*(1)\,\psi_c(1)}{\psi_v^*(1)\,\psi_v(1)}\,. \tag{A9}$$

If this charge is distributed uniformly with a value equal to $\rho(1, 1)$ throughout a spherical volume, the radius of the sphere is given by

$$\tfrac{1}{3}(4\pi r_0^3)\,\rho(1,1) = \rho(1)\,,$$

so that

$$r_0 = \left(\frac{3}{4\pi}\,\frac{\sum_{c_{11}} S_c\psi_v^*(1)\,\psi_c(1)/\psi_v^*(1)\,\psi_v(1)}{\sum_{c_{11}} \psi_c^*(1)\,\psi_c(1)} \right)^{1/3}\,. \tag{A10}$$

The potential of such a charge distribution at the center of the sphere is

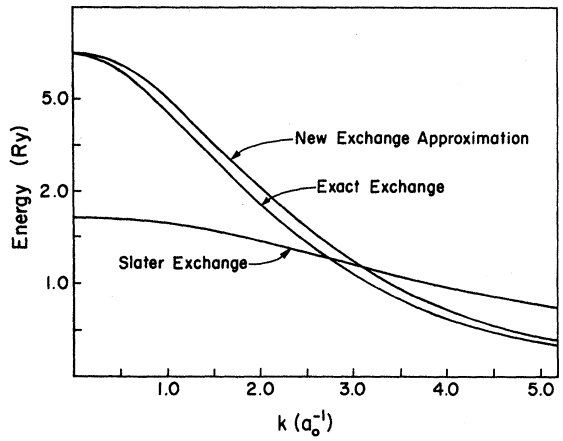

FIG. 8. Comparison of matrix elements of exact exchange. Slater exchange, and the new exchange approximation between one hydrogen orbital and a plane wave, as a function of the wave vector of the plane wave.

$$V_x = \int_0^{r_0} \frac{\rho(1,1)}{r}\, 4\pi r^2 dr = \frac{3}{2}\left[\frac{4\pi}{3}\, r_0^3 \rho(1,1)\right]\frac{1}{r_0} \,. \tag{A11}$$

In the manner of Slater, an average over occupied free-electron states leads to

$$V_x = \left\{-3\left(\frac{3}{4\pi}\right)^{1/3}\left[\sum_c |\psi_c(1)|^2\right]^{1/3}\right\}\left(\sum_c S_c \frac{\psi_c(1)}{\psi_v(1)}\right)^{2/3} . \tag{A12}$$

The first term is the Slater potential, the second is the nonorthogonality correction. Although this is more complicated than the Slater exchange (V_x depends not only on the ψ_c but on ψ_v), it does not involve an integration over a charge density. Hence matrix elements of V_x are, in general, easier to calculate than for exact exchange. In particular, if ψ_v and the ψ_c are spherically symmetrical, as in the case considered in this paper, the matrix elements are no more difficult to calculate than S_c. For simple choices of ψ_c and ψ_v, matrix elements of the exact form $\langle \psi_c | V_{xc} | \psi_v \rangle$ can be evaluated and compared with results obtained from the two approximations discussed above. With ψ_c of the hydrogenic form adopted in this paper and ψ_v respectively a plane wave and another hydrogenic wave function, the new approximation gives consistently much closer agreement with the exact results than does the Slater approximation. As an example, the results for ψ_v and a plane wave are shown in Fig. 8.

We note finally that the new exchange approximation is such that its usefulness is limited to cases in which ψ_c and ψ_v are spherically symmetrical. Otherwise terms like $Y_l^{|m|}(\theta_1, \phi_1)^{2/3}$ and $Y_l^{|m|}(\theta_1, \phi_1)^{-2/3}$ appear. The approximation of such terms is difficult, but may not be impossible.

APPENDIX B: LOW-TEMPERATURE TDS

The intensity of radiation scattered from a vibrating lattice in the kinematic approximation may be written[62]

$$I(\vec{S}) = |f_0|^2 e^{-2M}\left[I_0(\vec{S}) + I_1(\vec{S}) + \cdots\right] ,$$

where f_0 is the atomic scattering factor, $I_0(\vec{S})$ is the interference function of the rigid lattice for the scattering vector $\vec{S} = \vec{k} - \vec{k}_0$ ($\vec{k}$ and $\vec{k}_0$ are the scattered and incident wave vectors), and $I_1(\vec{S})$ is the single-phonon term in the TDS. This is the dominant phonon process and, in fact, may be a substantial fraction of the rigid-lattice scattering.[63] In the present discussion, we consider only this contribution to the TDS.

By assuming a Debye spectrum, McKinney, Jones, and Webb[52] have derived the following expression for TDS of low-energy electrons in the high-temperature limit ($T > \Theta_D$, where Θ_D is the Debye temperature):

$$I_1(\vec{S}) \propto (|\vec{S}|^2 kT/\rho) ,$$

where

$$\rho \equiv \frac{|\vec{S}_{11} - \vec{g}^{11}|}{\pi/d} .$$

The lattice spacing is given by d, and $\vec{S}_{11}$ and $\vec{g}^{11}$ are the components parallel to the surface of the scattering vector and the nearest reciprocal-lattice rod, respectively. Thus ρ is a measure of the fractional perpendicular distance from $\vec{S}$ to the nearest rod $\vec{g}_{11}$. The Be data were collected at 77 °K which is roughly one-tenth of the Debye temperature. It is appropriate then to use the low-temperature approximation ($T \to 0$) to the square of the amplitudes of the vibrational nodes in evaluating the TDS. When this is carried out, one finds

$$I_1(\vec{S}) \propto |\vec{S}|^2 k\Theta_D \left[\ln 4 - 2\ln\rho + \tfrac{1}{4}\rho^2\right] \quad \text{for } \rho < 1.$$

The quantity of interest, however, is the total amount of TDS which is accepted by the collector, together with the elastic component. This is, of course, a function of the collector aperature and is estimated as follows: The fraction of TDS accepted by the collector with aperature β is

$$f_{\mathrm{TDS}} = \int_0^{\beta} I_1(\vec{S})\, d\Omega \Big/ \int_0^{1} I_1(\vec{S})\, d\Omega ,$$

where β is defined as the ratio of radius of the collector to a collector which would intercept all the scattering in the Brillouin zone. Substitution of the low- and high-temperature values yields

$$f_{\mathrm{TDS}} \cong \begin{cases} \beta & \text{high temperature} \\ \beta^2[1 - 0.85\ln\beta] & \text{low temperature.} \end{cases}$$

A reasonable experimental aperature is $\beta \cong 0.1$. When substituted in the equation above, one finds that 10% TDS is accepted at high temperatures, whereas only 3% is accepted in the limit $T \to 0$.

*Work supported by the Advanced Research Projects Agency through the Materials Science Center at Cornell University, MSC Report No. 1411, and at Stony Brook by the Air Force Office of Scientific Research of the Office of Aerospace Research.

†Present address.

‡Present address: Kernforschungsanlage Jülich, IFF, 517 Jülich, Germany.

[1]H. Bethe, Ann. Physik 87, 55 (1928).

[2]P. M. Morse, Phys. Rev. 35, 1310 (1930).

[3]R. de L. Kronig and W. G. Penney, Proc. Roy. Soc. (London) A130, 499 (1931).

[4]C. Davisson and L. H. Germer, Phys. Rev. 30, 705 (1927); Proc. Natl. Acad. Sci. 14, 622 (1928).

[5]J. C. Slater, Phys. Rev. 51, 840 (1937).

[6]K. Molière, Ann. Physik 34, 461 (1939).

[7]E. G. McRae, J. Chem. Phys. 45, 3258 (1966); Surface Sci. 11, 479 (1968); 11, 492 (1968).

[8]K. Hirabayashi and Y. Takeishi, Surface Sci. 2, 509 (1966).

[9]K. Kambe, Z. Naturforsch. 22a, 322 (1967); 22a, 422 (1967).

[10]D. S. Boudreaux and V. Heine, Surface Sci. 8, 426 (1967).

[11]F. Hofmann and H. P. Smith, Jr., Phys. Rev. Letters 19, 1472 (1967); Phys. Rev. B 1, 2811 (1970).

[12]P. M. Marcus and D. W. Jepsen, Phys. Rev. Letters 20, 925 (1968).

[13]J. L. Beeby, J. Phys. C 1, 82 (1968).

[14]Y. H. Ohtsuki, J. Phys. Soc. Japan 24, 1116 (1968); 25, 481 (1968).

[15]J. B. Pendry, J. Phys. C 2, 1215 (1969); 2, 2273 (1969); 2, 2283 (1969).

[16]G. Capart, Surface Sci. 13, 361 (1969).

[17]C. M. K. Watts, J. Phys. C 1, 1237 (1969).

[18]P. J. Jennings, Surface Sci. 20, 18 (1970).

[19]V. Hoffstein and D. S. Boudreaux, Phys. Rev. Letters 25, 512 (1970).

[20]See, for example, I. H. Khan, J. P. Hobson, and R. A. Armstrong, Phys. Rev. 129, 1513 (1963); J. J. Lander and J. Morrison, J. Appl. Phys. 35, 3593 (1964). The form of the experimental results is shown schematically in Fig. 1(b).

[21]C. B. Duke and C. W. Tucker, Jr., Surface Sci. 15, 231 (1969); Phys. Rev. Letters 23, 1163 (1969).

[22]R. O. Jones and J. A. Strozier, Jr., Phys. Rev. Letters 22, 1186 (1969).

[23]Perhaps the most dramatic evidence for the existence of inelastic effects comes from epitaxial experiments, which show that the LEED pattern changes to that characteristic of the overlayer at coverages of a few monolayers. See, for example, N. J. Taylor, Surface Sci. 4, 161 (1966); C. A. Haque and H. E. Farnsworth, *ibid.* 4, 195 (1966); P. W. Palmberg and T. N. Rhodin, J. Chem. Phys. 49, 134 (1968); S. Andersson, I. Marklund, and J. Martinson, Surface Sci. 12, 269 (1968).

[24]J. J. Lander and J. Morrison, J. Appl. Phys. 34, 3517 (1963).

[25]P. W. Palmberg and W. G. Peria, Surface Sci. 6, 57 (1967).

[26]R. L. Gerlach and T. N. Rhodin, Surface Sci. 8, 1 (1967).

[27]M. G. Lagally and M. B. Webb, Phys. Rev. Letters 21, 1388 (1968).

[28]V. Heine, Proc. Phys. Soc. (London) 81, 300 (1963).

[29]J. M. Baker, Ph.D. thesis (Cornell University, 1970) (unpublished); J. M. Baker and J. M. Blakely (unpublished).

[30]The g_i^{11} vectors consist of all distinct projections of the three-dimentional reciprocal-lattice vectors of the crystal on the surface plane. They may be, as in Be basal plane, but are not necessarily the reciprocal-lattice vectors of the surface plane.

[31]See, for example, L. I. Schiff, *Quantum Mechanics* (McGraw-Hill, New York, 1955), Chap. VII.

[32]A. N. Gerritsen, *Handbuch der Physik* (Springer-Verlag, Berlin, 1956), Vol. 19, p. 137.

[33]W. A. Harrison, *Psuedopotentials in the Theory of Metals* (Benjamin, New York, 1966), Chap. 8.

[34]E. Holöien, Proc. Phys. Soc. (London) 68, 297 (1955).

[35]See, for example, A. Meyer and W. H. Young, Phys. Rev. 139, A401 (1965).

[36]H. Shull and P.-O. Löwdin, J. Chem. Phys. 25, 1035 (1956).

[37]*International Tables for X-ray Crystallography* (Kynoch Press, Birmingham, 1952), Sec. 3.3.

[38]J. C. Slater, Phys. Rev. 81, 385 (1951).

[39]A. Rosen and I. Lindgren, Phys. Rev. 176, 114 (1968).

[40]J. C. Slater, T. M. Wilson, and J. H. Wood, Phys. Rev. 179, 28 (1969).

[41]J. A. Strozier, Jr., Ph. D. thesis (University of Utah, 1966) (unpublished).

[42]T. L. Loucks and P. H. Cutler, Phys. Rev. 133, A819 (1964).

[43]A. O. E. Animalu, Phil. Mag. 11, 379 (1965).

[44]J. B. Pendry, J. Phys. C 1, 1065 (1968).

[45]S. Weinberg, Phys. Rev. 130, 776 (1963).

[46]R. J. Austin, V. Heine, and L. J. Sham, Phys. Rev. 127, 276 (1962).

[47]J. H. Tripp, P. M. Everett, W. L. Gordon, and R. W. Stark, Phys. Rev. 180, 669 (1969).

[48]From Ref. 46. Calculated using the potential of A. O. E. Animalu and V. Heine, Phil. Mag. 12, 1249 (1965).

[49]B. I. Lundqvist, Phys. Status Solidi 32, 273 (1969).

[50]See, for example, J. M. Ziman, *Principles of the Theory of Solids* (Cambridge U.P., Cambridge, England, 1964), p. 54 ff.

[51]D. L. Huber, Phys. Rev. 153, 772 (1967).

[52]J. T. McKinney, E. R. Jones, and M. B. Webb, Phys. Rev. 160, 523 (1967).

[53]B. I. Lundqvist (private communication).

[54]F. Bassani, J. Robinson, B. Goodman, and J. R. Schrieffer, Phys. Rev. 127, 1969 (1962).

[55]L. Hedin and S. Lundqvist, Solid State Phys. 23, 1 (1969).

[56]The present results incorporate some refinements not included in the short report presented earlier [J. A. Strozier, Jr. and R. O. Jones, Phys. Rev. Letters 25, 516 (1970)]. Specifically, the Debye-Waller factor is included and the exact expression for $B_1(1, i)[2]$ is used [Eq. (25)]. A close approximation to the exact result, involving the neglect of the final term in this expression, was used earlier. The inclusion here results in changes at low energies where the imaginary part of the self-energy changes rapidly. A numerical error in the Hartree term has also been rectified.

[57]Based primarily on Ref. 41.

[58]R. Gáspár, Acta Phys. Hung. 3, 263 (1954).

[59]W. Kohn and L. J. Sham, Phys. Rev. 140, A1133 (1965).

[60]F. Herman, J. P. Van Dyke, and I. B. Ortenburger,

Phys. Rev. Letters 22, 807 (1969).
[61]D. A. Liberman, Phys. Rev. 171, 1 (1968).
[62]See, for example, A. A. Maradudin, E. W. Montroll, and G. H. Weiss, *Lattice Dynamics in the Harmonic Approximation* (Academic, New York, 1963), p. 24 2ff.
[63]C. B. Walker, Phys. Rev. 103, 547 (1956).

PHYSICAL REVIEW B VOLUME 3, NUMBER 10 15 MAY 1971

Momentum Distribution and Pair Correlation of the Electron Gas at Metallic Densities*

John Lam†
Division of Chemistry, National Research Council of Canada, Ottawa 7, Canada
(Received 11 December 1970)

The momentum-distribution and pair-correlation functions of the electron gas at metallic densities are calculated by means of an expression of the ground-state energy derived in a previous paper. Numerical studies of the momentum distribution show that even at metallic densities most of the electrons are still inside the Fermi sphere and that the Fermi surface persists. The effect of the exchange processes at metallic densities is found to pull the electrons back inside the Fermi sphere and to increase the discontinuity at the Fermi surface, which is the opposite effect to that at high density. The behavior of the pair-correlation functions indicates that at short distances the present results overestimate the correlation of antiparallel spins but underestimate that of parallel spins. On the whole, there is considerable improvement over the corresponding results in the random-phase approximation.

I. INTRODUCTION

In a previous paper[1] we formulated an approach to the correlation problem of the electron gas at metallic densities. The starting point of this approach is the transition from the paramagnetic fermion-state space to a boson-state space, by means of a transformation first introduced by Usui[2] to study the effect of exchange processes on the properties of a spinless electron gas at high density. Under this transformation, an electron-hole pair goes over into an ideal boson:

$$a^{\dagger}_{\vec{P}\sigma}\, a_{\vec{p}\sigma} \to C^{\dagger}_{\vec{p}\sigma}(\vec{P}-\vec{p}), \qquad P>p_F,\quad p<p_F\,. \tag{1.1}$$

The electron Hamiltonian H_F is mapped into a boson Hamiltonian of the form

$$H_B = H_0 + H_2 + H_3 + H_4\,. \tag{1.2}$$

Here H_0 is a c number identical to the ground-state energy in the Hartree-Fock approximation; H_2, H_3, and H_4 are, respectively, quadratic, cubic, and quartic in boson creation and annihilation operators. The ensuing calculations in Ref. 1 are based on two types of approximations. The first consists of the harmonic approximation in which H_3 and H_4 are assumed small and discarded. Then H_2 can be separated into two mutually independent parts describing the singlet and triplet states of an electron-hole pair:

$$H_2 = H^{(1)} + H^{(3)}\,. \tag{1.3}$$

The second type of approximation is employed to diagonalize these parts, and consists roughly in replacing the matrix elements of exchange processes by their averages. The result of these approximations is equivalent to taking as the singlet Hamiltonian the expression

$$H^{(1)} = \sum_{\vec{q}\vec{p}} \omega_{\vec{p}}(\vec{q})\, A^{\dagger}_{\vec{p}}(\vec{q})\, A_{\vec{p}}(\vec{q}) + \frac{1}{\Omega}\sum_{\vec{q}\vec{p}\vec{p}'}\{2F(\vec{q})\, A^{\dagger}_{\vec{p}}(\vec{q})\, A_{\vec{p}'}(\vec{q}) + G(\vec{q})[A^{\dagger}_{\vec{p}}(\vec{q})\, A^{\dagger}_{-\vec{p}'}(-\vec{q}) + \text{H.c.}]\}\,. \tag{1.4}$$

The notations in this paper are as in Ref. 1. In particular,

$$\omega_{\vec{p}}(\vec{q}) = \epsilon_{\vec{p}+\vec{q}} - \epsilon_{\vec{p}}\,,$$
$$F(\vec{q}) = V(\vec{q}) + f(\vec{q})\,,$$
$$G(\vec{q}) = V(\vec{q}) + g(\vec{q})\,. \tag{1.5}$$

Here $\epsilon_{\vec{p}}$ is the electron kinetic energy and $V(\vec{q})$ is the direct Coulomb potential. $f(\vec{q})$ and $g(\vec{q})$ are a pair of effective potentials expressible in terms of certain exchange matrix elements. They are defined in Eq. (5.7) and plotted in Fig. 2 of Ref. 1. The ground-state energy of $H^{(1)}$ is the singlet contribution to the correlation energy. It is given by

$$E^{(1)}_{\text{corr}} = \frac{1}{4\pi}\sum_{\vec{q}}\int_{-\infty}^{\infty} du\,[\ln\epsilon(\vec{q}, iu) - \Pi_1(\vec{q}, u)]\,, \tag{1.6}$$

where

$$\epsilon(\vec{q}, iu) = 1 + \Pi_1(\vec{q}, u) + \Pi_2(\vec{q}, u)\,,$$